In-situ Realtime Monitoring of Nanoscale Gold Electroplating Using MEMS Liquid Cell Operating in TEM

Minoru Egawa, Tadashi Ishida, Laurent Jalabert, Hiroyuki Fujita

In-situ Realtime Monitoring of Nanoscale Gold Electroplating Using MEMS Liquid Cell Operating in TEM

Minoru Egawa,[1] Tadashi Ishida,[1,2*] Laurent Jalabert[3,4] and Hiroyuki Fujita.[1]

[1]*Institute of Industrial Science, University of Tokyo, Meguro, Tokyo, 153-8505, Japan*

[2]*Graduate school of Science and Technology, Tokyo Institute of Technology, Yokohama, Kanagawa, 225-8503, Japan*

[3]*LIMMS/CNRS-IIS (UMI 2820), Institute of Industrial Science, University of Tokyo, Meguro, Tokyo, 153-8505, Japan*

[4]*CNRS, LAAS, 7 avenue du colonel Roche, F-31400 Toulouse, France; University of Toulouse, LAAS, F-31400 Toulouse, France*

**Corresponding author : Tadashi Ishida (*Electronic mail: ishida.t.ai@m.titech.ac.jp)

Abstract

The dynamics of nanoscale electroplating between gold electrodes was investigated using a micro fabricated liquid cell mounted in a scanning transmission electron microscope. The electroplating was recorded *in-situ* for 10 minutes with a spatial resolution higher than 6 nm. At the beginning of the electroplating, gold spike-like structures of about 50 nanometers in size grew from an electrode, connected gold nanoclusters around them, and form three dimensional nanoscale structures. We visualized the elementary process of the gold electroplating, and believe that the results lead to the deeper understanding of electroplating at the nano scale.

Main text

Observing in-liquid phenomena with nanoscale resolution is challenging, but highly required in material science, chemistry, biology, and nanoelectronics. One of the large research fields of the in-liquid observation with nanoscale resolution is electrochemistry, which covers material corrosion, electroplating, batteries, capacitors, and biosensors. In electrochemistry, dendrites, which are sharp metallic protrusions formed during electrodeposition, can be very interesting candidate for sensing applications because of the high surface to volume ratio, but represent a serious reliability issue in Li-ion[1] and lead-acid[2] batteries. In microelectronics, with the recent development of "system-on-package" using electroplated through-silicon vias (TSVs)[3,4], dendrites formation should be also avoided to prevent high local electric fields.[5,6] The roughness of a thin film formed by the dendrites is even more critical in molecular electronics as in the same order of magnitude than the size of sample molecules, as well as the fabrication of a nanogap by the conventional lithography and etching methods. Electroplating represents an elegant and complementary approach as a narrowing process of a nanogap until it reaches the critical size of a single molecule.[7,8] However the correlation between the conditions of electroplating to form such a nanogap relies on empirical results obtained by successive post-processing observations and process adjustments. Therefore, it is important to study the elementary process of the electroplating at the nano scale, which will define the deposition geometry such as dendrite. For this purpose, many in-liquid *in-situ* monitoring techniques have been developed, such as in-liquid atomic force microscope (AFM)[9] and scanning ion conductive microscopy (SICM)[10]. The electric field

distribution around sharp tips can stir the electroplating solution adding more complex phenomena to the in-liquid growth and low imaging time. To overcome those problems, in-liquid transmission electron microscopy (TEM)[11] has become an emerging technique with new technological challenges since high resolution requires operating in high vacuum conditions.

In-liquid TEM techniques started from 1944,[12] and have been recently improved with updated technology of advanced micro-electro-mechanical systems (MEMS) fabrication to create liquid cell for TEM, also called LCTEM. LCTEM allowed for the first time the observation of *in-situ* nanoscale nucleation and growth of Cu by electroplating.[11] LCTEM is based on the assembly of two silicon chips having thin suspended membranes for electron transparency and mechanical rigidity. A sample and its surrounded liquid environment are manually introduced via inlets and outlets into a cavity formed by a silicon dioxide spacer of typically 1 µm thick or less.[12,13] The chips can be assembled and sealed with epoxy[2,12] or by wafer bonding[13] to operate in high vacuum conditions. Suspended nitride membranes with the thickness in the range from 30 nm to 100 nm are commonly optimized considering a tradeoff between mechanical rigidity and electron transparency. There are trials to replace the membrane with graphene to improve the imaging resolution.[14-16] Commercially available LCTEM increases the interest for in-liquid nanoscale electrochemical researches,[17,18] especially to reveal the mechanisms of nanoparticle growth from ligand/metal self-assembly,[19] the role of a hydration layer in the formation of aggregates[20] or also the nucleation of conjugated polymer such as the organic poly(3,4-ethylenedioxythiophene) (PEDOT) by electrochemical process.[21] However, LCTEM suffers from the vibration, dose limitation of electron beam irradiation, which prevent nanoscale observation of electroplating without other electrodeposition effects for a long duration.

Here, we developed a simple electrochemical MEMS liquid cell for *in-situ* observing a nanogap narrowing process induced by electroplating between sharp opposing tips. The working principle is similar to the one reported recently for monitoring Li deposition on gold electrodes,[22] and has fully-integrated electrodes compared to previous work.[12] Our electrochemical MEMS liquid cell is easily compatible with a homemade scanning TEM (STEM) holder. The holder has 5 electrical bumps mechanically contacting the pads on the MEMS for easy device exchanges without any wire bonding.[23] The MEMS liquid cell is introduced into a specimen chamber of STEM (HD-2300, Hitachi) with 200 kV in acceleration voltage using a STEM holder. The operating condition is high vacuum (~10^{-5} Pa), an electron beam current of ~30 pA, and a frame rate of 30 fps. The electron beam current is 200 times lower, and the frame rate is 15 times faster as compared to Ref. 22, respectively, which are expected to avoid electron beam assisted gold dendrites growth.[24] The high resolution and longer visualization duration are achieved by the suppression of the environmental-coupled vibrations using double-fixing mechanism of the STEM holder and fixing wirings on an anti-vibration stage. Via feedthroughs and cables that are fixed on an anti-vibration stage, the MEMS liquid cell is electrically connected with a source measurement unit of a semiconductor parameter analyzer (B1500, Agilent). Using the MEMS liquid cell, we *in-situ* STEM observed the temporal change in shape of gold electrodes with a spatial resolution of 6 nm during an electroplating duration of 10 minutes.

Figure 1 shows the MEMS liquid cell for the visualization of electroplating at the nanoscale. The MEMS liquid cell is fabricated by assembling a window chip and an electrode chip. The chips have 80-nm-thick silicon nitride membranes of 200 µm x 200 µm for the electron transparent window. The window chip has inlets and outlets to introduce electroplating solution. The electrode chip has gold opposing tips and a counter electrode (located 400 µm away from the tips) made of Cr/Au (5 nm/50 nm) patterned by electron beam lithography (F5112+VD01, ADVANTEST), and a 2-µm-thick patterned photoresist spacer (Shipley S1818) over electrodes that defines a cavity of 1.2 µl. The initial gap between the opposing tips is 2.4 µm.

The chips are optically aligned and sealed with ultra violet (UV) cured epoxy resin. The cavity is filled with a homemade gold electroplating solution through 3 inlets and outlets made on the window chip. The gold electroplating solution of 25.6 mM in gold concentration (the mixture of iodine tincture, L(+)-ascorbic acid, known as vitamin C, and gold) is introduced from the inlet of the window chip. The L(+)-ascorbic acid replaces toxic cyanide compounds and works as a reducing agent of I_3^-, which oxidize and dissolve gold electrodes.[25] The inlets and outlets are then sealed with UV cured epoxy to keep the solutions away from the vacuum in STEM.

Before starting the visualization of the electroplating, the influence on the morphological change of the electrodes caused by the electron beam itself should be discussed. The morphological changes are observed at 30 frames/sec at magnification of 40 k using an electron beam current of typically i_e=30 pA. The image size is 640 x 480 pixels. One pixel size in the image is 6 nm x 6 nm. Electron dose per frame is calculated by

$$D_f = \frac{i_e t_{1f}}{qS} = \frac{30 \times 10^{-12} \times 33 \times 10^{-3}}{1.6 \times 10^{-19} \times 11 \times 10^{6}} = 0.56\ electrons/nm^2$$

where q is the charge of the electron, S the frame size (nm^2), t_{1f} the time per frame (30 frames per seconds).[26] Dividing the dose per frame by the scanning time gives a dose rate ($\dot{d}$) of 17 electrons/nm^2s = $0.76 \times 10^6\ Gy/s$ (unit used in radiation chemistry).[27] Such a dose rate is 4 orders of magnitude lower than the threshold dose rate of 10^9 Gy/s to induce gold nucleation in water solution under electron irradiation. We optimized a high frame rate together with a low magnification observation (40 k) to limit the influence of electron irradiation on the radiolysis of the solution.[28] Compared to water solution that has been intensively studied, radiolysis of an electroplating solution might give more complex chemistry that might lower the dose rate threshold. Nucleation is observed for high dose rate at magnification over 250 k.[28] Possible accumulation of charges on the nitride membrane and also charges created by the radiolysis of the plating solution can be dissipated through the grounded electrode on the bottom chip. Therefore, under our experimental conditions, the contribution of electron-beam irradiation to the morphological change of electrodes can be neglected compared to the electroplating process.

We *in-situ* visualize the dynamic change of the opposing electrodes caused by the electroplating, as shown on Figure 2 displaying a sequence of images extracted from a real time video[29]. The initial condition of a tip of the opposing electrodes is shown in Fig. 2(a). Nanoscale clusters from 50 nm to 300 nm in diameter surround a tip of a gold electrode, which may be formed due to the etching of the electrode by the gold electroplating solution. We applied 0.5 V between a counter electrode and the opposing electrodes to start the electroplating.[29] The applied voltage should be less than 1.1 V in order to suppress electrolysis of water. This is because bubbles of hydrogen[26,30] and oxygen are formed over the threshold voltage, and then the electroplating solution changed into gas phase, resulting in thousands times increase in volume that can damage the thin suspended membrane. Once the voltage of 0.5 V was applied, electrical current of 1 μA passed between the electrodes. Gold ions were precipitated on the gold electrodes according to the chemical reaction[26] of $2[AuI_4]^- + I^- \leftrightarrow 2Au + 3I_3^-$. At the beginning, the electrode and the surrounding clusters gradually became larger in random direction by the precipitation. Some of the precipitated structures became tiny spike-shaped. One of the spike-like structures was 49 nm in width and 43 nm in height. They grew from the edge of the electrode. The spike-like structures grew to 50 nm in width and 115 nm in height after 1 minute from the appearance of the spike-like structures. Some of them reached the surrounding nanoscale clusters. The electrode and clusters were connected with the spike-like structures (Fig. 2(b)). Once the connections were formed between the electrode and the surrounding clusters, other spike-like structures appeared from the clusters, without expanding in the direction of the electric field, forming three-dimensional structures (darker areas in Fig 2(c-e)). Finally, the

electroplating process was terminated (Fig. 2(f)). During the electroplating, the current was constant at 1 μA. In Fig. 2, the spatial resolution of STEM imaging in liquid was 6 nm, defined as the minimum gap measured between two distinct clusters. The mechanism of the spike-like formation observed from Fig. 2(c) mainly resulted from initial gold particles and polycrystalline clusters, irregular in shape and size[31]. However the spikes did not expand to form regular dendrites possibly because of the low electric field[32,33] and the absence of surfactants[34].

The area of the electroplated gold structure is measured from the dark area in the image (Fig. 3). The rate of the electroplating area increased from 0 to 2 min. It reached 1.5×10^{-1} μm^2/min at 2 min. From 2 min to 11 min, the rate gradually decreased down to 1.8×10^{-2} μm^2/min. At 11 min 30 s, we could not observe any precipitation. The shapes of the micro gap between the opposing electrodes were compared between before and after the electroplating using Z-contrast images (Fig. 4). The electrodes before the electroplating had cracks on the structure and were surrounded by the nanoscale clusters (Fig. 4(a)). The gap was 2.1 μm as patterned. After the electroplating for 11 min 30 s, the electrodes had many spike-like structures on the edge (Fig. 4(b)). The gap became 1.4 μm due to the electroplating of gold. The average rate of gold electroplating at the gap is calculated to be 1 nm/s. The maximum growth is 351 nm at the gap of the tips, and the average growth is almost 210 nm at the edges of the electrodes.

The precipitated volume of gold on the edge of all the electrodes facing on the solution is 1.4×10^3 μm^3. This volume of the precipitated gold corresponds to 1.4×10^{-10} mol, with the density of 1.9×10^4 kg/m^3 and an atomic weight of 197. The concentration of gold ions in the electroplating solution is 2.8×10^{-10} mol. With the comparison of the amounts of gold, the gold in the electroplating solution still remained without precipitating. We believe that the rate of electroplating became slow due to the following mechanism. At the initial stage, gold ions inside the solution are attracted to the electrodes by the electric field, resulting in the formation of spike-like structures on the electrodes that could act as precursor of dendrite growth. As the electroplating proceeded, the gold ions gradually became sparse by the precipitation on the electrodes. The gold ions were transported from the counter electrode to the opposing tips driven by a low electric field (2kV/cm) and diffusion. However, the consumption due to the electroplating is faster than the supply due to the slow transportation of gold ions. Considering the balance between efflux and influx of gold ion around the electrodes, the concentration of the gold ions near the electrodes decreased. Therefore, the rate of the electroplating decreased. The same situation may occur at the bottom of narrow and deep via holes, the supply of the gold ions should be well designed to maintain the rate of electroplating.

We have developed the MEMS liquid cell for *in-situ* observation of the nanoscale gold electroplating process. The growth of the gold electrode due to the electroplating was visualized in real-time with a spatial resolution higher than 6 nm. Low electric field and the absence of surfactant prevent the spike-like structures to expand and form regular dendrite structures. The electroplating growth rate is possibly limited by the reactivity of minority species in the microliter volume of solution. We believe that the experimental set-up will be helpful to improve the electroplating process for highly qualified TSV, redox-based resistive switching memories[35], as well as for improving nanogap formation for molecular electronics and bio-sensing applications.

This work was supported by JSPS KAKENHI Grant Number 26246009 and 15H05416. The photolithography mask was made using the 8-inch EB writer F5112+VD01 donated by ADVANTEST Corporation to the VLSI Design and Education Center (VDEC, The University of Tokyo). The electron transparent membrane was made in Tohoku University Hands-on-access fab. in Micro System Integration Center (μSIC, Tohoku University).

References

1 Z. Guo, J. Zhu, J. Feng, and S. Du, *RSC Adv.* **5**, 69514 (2015).

2 M. Sun, H.-G. Liao, K. Niu, and H. Zheng, *Sci. Rep.* **3**, 3227 (2013).

3 Y. Feng, and S. L. Burkett, *J. Vac. Sci. Technol. B*, **33** 0220004 (2015).

4 T. Chen, J. Sun, and R. Yan, Proceedings of the 16th International Conference on Electronic Packaging Technology, Changsha, China, 11-14 August 2015 (IEEE, New York) pp 860-865 (2015).

5 N. Khan, V.S. Rao, S. Lim, H.S. We, V. Lee, X. Zhang, E.B. Liao, R. Nagarajan, T.C. Chai, V. Kripesh, and J.H. Lau, *IEEE T. Compon. Pack. T.* **33**, 3 (2010).

6 P.C. Andricacos, C. Uzoh, J.O. Dukovic, J. Horkans, and H. Deligianni, *IBM J. Res. Dev.* **42**, 567 (1998).

7 A. Umeno and K. Hirakawa, *Appl. Phys. Lett.* **86**,143103 (2005).

8 L. D. L. S. Valladares, L. L. Felix, A. B. Dominguez, T. Mitrelias, F. Sfigakis, S.I. Khondaker, C.H.W. Barnes, and Y. Majima, *Nanotechnology* **21**, 445304 (2010).

9 T. Tian, B. Singhana, L. E. E-Frankline, X. Zhai, T. R. Lee, and C. Garno, *Beilstein J. Nanotechnol.* **5**, 26-35 (2014).

10 P. K. Hansma, B. Drake, O. Marti, S. A. C. Gould, C. B. Prater, *Science*, **243**, 641-643 (1988).

11 M.J. Williamson, R.M. Tromp, P.M. Vereecken, R. Hull, and F.M. Ross, *Nat. Mater.* **2**, 532 (2003).

12 I.M. Abrams and J.W. McBain, *Science* **100**, 273 (1944).

13 J.M. Grogan and H.H. Bau, *J. Microelectromech. Syst.* **19**, 885 (2010).

14 J.M. Yuk, J. Park, P. Ercius, K. Kim, D.J. Hellebusch, M.F. Crommie, J.Y. Lee, A. Zettl, and A.P. Alivisatos, *Science* **336**, 61 (2012).

15 Q. Chen, J.M. Smith, J. Park, K. Kim, D. Ho, H.I. Rasool, A. Zettl, and A.P. Alivisatos, *Nano Lett.* **13**, 4556 (2013).

16 C. Wang, Q. Qiao, T. Shokuhfar, and R.F. Klie, *Adv. Mater.* **26**, 3410 (2014).

17 see http://www.protochips.com/products/poseidon.html for commercial liquid cell from Protochips.

18 see http://hummingbirdscientific.com/products/liquid/ for commercial liquid cell from Hummingbird.

19 E. Firlar, S. Çınar, S. Kashyap, M. Akinc, and T. Prozorov, *Sci. Rep.* **5**, 9830 (2015).

20 J.P. Patterson, P. Abellan, M.S. Denny Jr., C. Park, N.D. Browning, S.M. Cohen, J.E. Evans, and N.C. Gianneschi, *J. Am. Chem. Soc.* **137**, 7322 (2015).

21 J. Liu, B. Wei, J.D. Sloppy, L. Ouyang, C. Ni, and D.C. Martin, *ACS Macro Lett.* **4**, 897 (2015).

22 R.L. Sacci, N.J. Dudney, K.L. More, L.R. Parent, I. Arslan, N.D. Browning, and R.R. Unocic, *Chem. Commun.* **50**, 2104 (2014).

23 A.J. Leenheer, J.P. Sullivan, M.J. Shaw, and C.T. Harris, *J. Microelectromech. Syst.* **24**, 1061 (2015).

24 T. Kraus and N. de Jonge, Langmuir, *Langmuir* **29**, 8427 (2013).

25 Y. Nakao, and K. Sone, *Chem. Commun.* **8**, 897 (1996).

26 P. Abellan, T.J. Woehl, L.R. Parent, N.D. Browning, J.E. Evans, and I. Arslan, *Chem. Commun.* **50**, 4873 (2014).

27 D. Alloyeau, W. Dachraoui, Y. Javed, H. Belkahla, G. Wang, H. Lecoq, S. Ammar, O. Ersen, A. Wisnet, F. Gazeau, and C. Ricolleau, *Nano Lett.* **15**, 2574 (2015).

28 N.M. Schneider, M.M. Norton, B.J. Mendel, J.M. Grogan, F.M. Ross, and H.H. Bau, *J. Phys. Chem. C* **118**, 22373 (2014).

29 See supplemental material at [URL] for e-beam induced gold formation at high magnification, *in-situ* STEM video of electroplating process, and electrical setup.

30 Y. Liu and S.J. Dillon, *Chem. Commun.* **50**, 1761 (2014).

31 J. Xiao and L. Qi, *Nanoscale* **3**, 1383-1396 (2011).

32 Y. Hu, N. Pan, K. Zhang, Z. Wang, H. Hu, and Xi Wang, *Phys. Stat. Sol. (a)*, **204**, 3398-3404 (2007).

33 C. Motoc, *J. Cryst. Growth*, **12**, 309-315 (1972).

34 X. Han, D. Wang, J. Huang, D. Liu, T. You, *J. Colloid Interface Sci.* **354**, 577-584 (2011).

35 R. Waser, R. Dittmann, G. Staikov and K. Szot, *Adv. Mat.* **21**, 2632-2663 (2009)

Figures

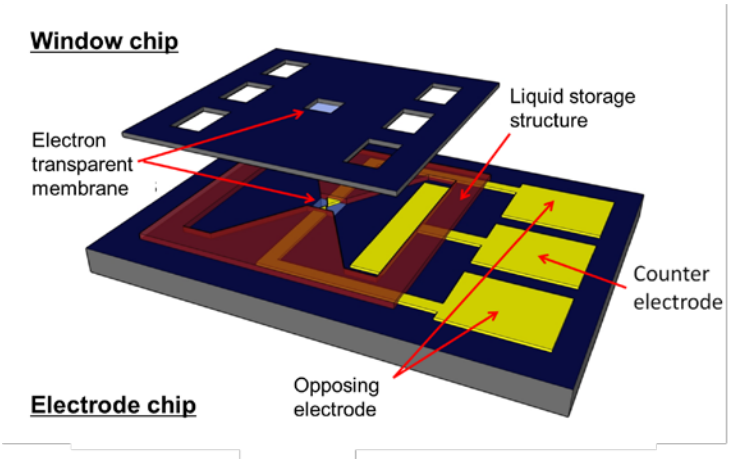

FIG. 1. (color online) Schematic illustration of the MEMS liquid cell with integrated electrodes and photoresist spacer.

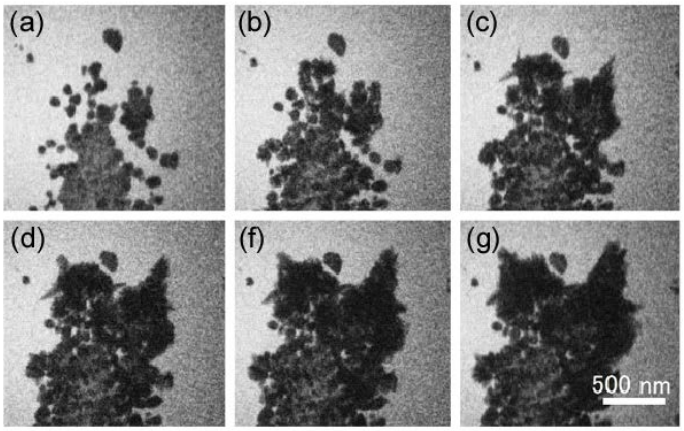

FIG. 2. Sequence of STEM images extracted from real-time video (see supplemental materials) showing the morphological change of the apex of the gold electrode during electroplating, at (a) 0 min, (b) 2 min, (c) 4 min, (d) 6 min, (e) 8 min, and (f) 10min. (see Supplementary Movie 1)

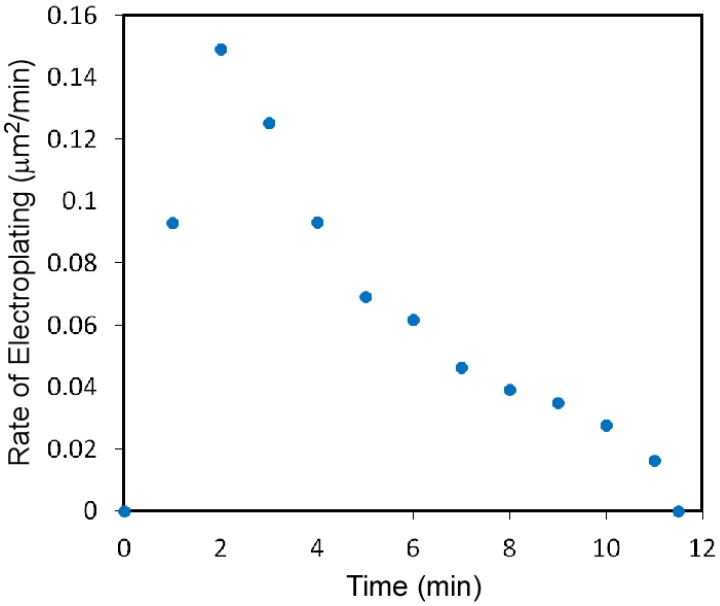

FIG. 3. Growth rate defined as the projected electroplated area as a function of time.

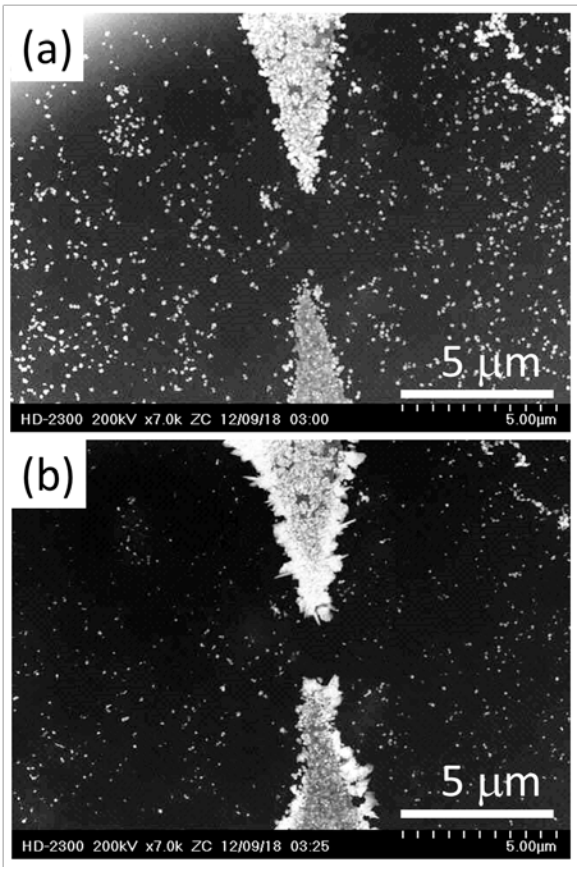

FIG. 4. Z-contrast images of the apex of gold electrodes (a) before and (b) after electroplating, showing the narrowed gap.